



1 **Research article**

2 **Title**

3 Spatially asynchronous changes in strength and stability of terrestrial net ecosystem  
4 productivity

5 **Running title**

6 Spatial variability in terrestrial NEP

7 **Authors**

8 Erqian Cui<sup>1,2</sup> (eqcui@stu.ecnu.edu.cn)

9 Chenyu Bian<sup>1,2</sup> (cybian@stu.ecnu.edu.cn)

10 Yiqi Luo<sup>3</sup> (yiqi.luo@nau.edu)

11 Shuli Niu<sup>4,5</sup> (sniu@igsnr.ac.cn)

12 Yingping Wang<sup>6</sup> (Yingping.Wang@csiro.au)

13 Jianyang Xia<sup>1,2,\*</sup> (jyxia@des.ecnu.edu.cn)

14 **Affiliations**

15 <sup>1</sup>Zhejiang Tiantong Forest Ecosystem National Observation and Research Station, Shanghai  
16 Key Lab for Urban Ecological Processes and Eco-Restoration, School of Ecological and  
17 Environmental Sciences, East China Normal University, Shanghai 200241, China;

18 <sup>2</sup>Research Center for Global Change and Ecological Forecasting, East China Normal  
19 University, Shanghai 200241, China;

20 <sup>3</sup>Center for ecosystem science and society, Northern Arizona University, Arizona, Flagstaff,  
21 AZ 86011, USA.

22 <sup>4</sup>Key Laboratory of Ecosystem Network Observation and Modeling, Institute of Geographic  
23 Sciences and Natural Resources Research, Chinese Academy of Sciences, Beijing, China;

24 <sup>5</sup>University of Chinese Academy of Sciences, Beijing, China;

25 <sup>6</sup>CSIRO Oceans and Atmosphere, PMB 1, Aspendale, Victoria 3195, Australia.

26 **Correspondence**

27 Jianyang Xia, School of Ecological and Environmental Sciences, East China Normal  
28 University, Shanghai 200241, China.

29 Email: jyxia@des.ecnu.edu.cn

30 **Key words**

31 Net ecosystem productivity, spatial asynchronous, CO<sub>2</sub> uptake and release, local indicators,  
32 model



33 **Abstract**

34 Multiple lines of evidence have demonstrated the persistence of global land carbon (C) sink  
35 during the past several decades. However, both annual net ecosystem productivity (NEP) and its  
36 inter-annual variation ( $I\Delta V_{NEP}$ ) keep varying over space. Thus, identifying local indicators for  
37 the spatially varying NEP and  $I\Delta V_{NEP}$  is critical for locating the major and sustainable C sinks  
38 on the land. Here, based on a machine-learning-derived database, we first showed that the  
39 variations of NEP and  $I\Delta V_{NEP}$  are spatially asynchronous. Then, based on daily NEP  
40 observations from eddy covariance sites, we found robust logarithmic correlation between  
41 annual NEP and ratio of total  $CO_2$  exchanges during net uptake ( $U$ ) and release ( $R$ ) periods  
42 (i.e.,  $U/R$ ). The cross-site variation of mean annual NEP can be linearly indicated by  $\ln(U/R)$ ,  
43 while the spatial distribution of  $I\Delta V_{NEP}$  was well indicated by the slope (i.e.,  $\beta$ ) of the  
44 demonstrated logarithmic correlation. Among biomes, for example, forests and croplands had  
45 the largest  $U/R$  ratio ( $1.06 \pm 0.83$ ) and  $\beta$  ( $473 \pm 112 \text{ g C m}^{-2} \text{ yr}^{-1}$ ), indicating the highest NEP  
46 and  $I\Delta V_{NEP}$  in forests and croplands, respectively. We further showed that the spatial variations  
47 of NEP and  $I\Delta V_{NEP}$  were both underestimated by the machine-learning-based and  
48 process-based global models. Overall, this study underscores the asynchronously changes in  
49 the strength and stability of land C sinks over space, and provides two simple local indicators  
50 for their intricate spatial variations. These indicators could be helpful for locating the  
51 persistent terrestrial C sinks and provides valuable constraints for improving the simulation of  
52 land-atmospheric C exchanges.

53



54 **1. Introduction**

55 Terrestrial ecosystems reabsorb about one-quarter of anthropogenic CO<sub>2</sub> emission (Ciais et al.,  
56 2019) and are primarily responsible for the recent temporal fluctuations of the measured  
57 atmospheric CO<sub>2</sub> growth rate (Randerson, 2013; Le Quéré et al., 2018). However, evidence  
58 based on eddy-flux measurements (Baldocchi, Chu, & Reichstein, 2018; Rödenbeck, Zaehle,  
59 Keeling, & Heimann, 2018), aircraft atmospheric budgets (Peylin et al., 2013), and  
60 process-based model simulations (Poulter et al., 2014; Ahlstrom et al., 2015) has shown a large  
61 spatial variability in net ecosystem productivity (NEP) on the land. The elusive variation of  
62 terrestrial NEP over space refers to both of the dramatic varying mean annual NEP and the  
63 divergent inter-annual variability (IAV) in NEP (i.e., IAV<sub>NEP</sub>; usually quantified as the standard  
64 deviation of annual NEP) across space (Baldocchi, Chu, & Reichstein, 2018; Marcolla,  
65 Rödenbeck, & Cescatti, 2017). The mean annual NEP is related to the strength of carbon sink  
66 of a specific ecosystem (Randerson, Chapin III, Harden, Neff, & Harmon, 2002; Luo, & Weng,  
67 2011; Jung et al., 2017), while IAV<sub>NEP</sub> characterizes the stability of such carbon sink (Musavi  
68 et al., 2017). Thus, whether and how NEP and IAV<sub>NEP</sub> change asynchronously over the space  
69 is important for predicting the future locations of carbon sinks on the land (Yu et al., 2014; Niu  
70 et al., 2017).

71 The NEP in terrestrial ecosystems is determined by two components, including vegetation  
72 photosynthesis and ecosystem respiration (Reichstein et al., 2005). Because there is a strong  
73 covariance between photosynthesis and respiration over space (Baldocchi, Sturtevant, &  
74 Contributors, 2015; Biederman et al., 2016), their relative difference could determine the  
75 spatial variation of NEP. Many previous analyses have attributed the IAV<sub>NEP</sub> at the site level to  
76 the different sensitivities of ecosystem photosynthesis and respiration to environmental  
77 fluctuations among years (Gilmanov et al., 2005; Reichstein et al., 2005; Musavi, 2017). For  
78 example, some studies have reported that IAV<sub>NEP</sub> is more associated with variations in  
79 photosynthesis than carbon release (Ahlstrom et al., 2015; Novick, Oishi, Ward, Siqueira,  
80 Juang, & Stoy, 2015; Li et al., 2017), whereas others have indicated that respiration is more  
81 sensitive to anomalous climate variability (Valentini et al., 2000; von Buttlar et al., 2017).  
82 Alternatively, the annual NEP of a given ecosystem can be defined numerically as the balance



83 between the CO<sub>2</sub> uptake and release processes (Gray et al., 2014), which are more direct  
84 components for NEP (Fu et al., 2019). It is still unclear whether ecosystem CO<sub>2</sub> uptake and  
85 release could be integrated into some simple indicators for the spatially varying NEP and  
86 IAV<sub>NEP</sub> in terrestrial ecosystems.

87 Conceptually, the total CO<sub>2</sub> uptake flux ( $U$ ) is determined by the length of CO<sub>2</sub> uptake  
88 period ( $CUP$ ) and the CO<sub>2</sub> uptake rate, while the total CO<sub>2</sub> release flux ( $R$ ) depends on the  
89 length of CO<sub>2</sub> release period ( $CRP$ ) and the CO<sub>2</sub> release rate (Fig. 2b). The variations of NEP  
90 thus should be innovatively attributed to these decomposed components. A strong spatial  
91 correlation between mean annual NEP and length of CO<sub>2</sub> uptake period has been reported in  
92 evergreen needle- and broad-leaved forests (Churkina, Schimel, Braswell, & Xiao, 2005;  
93 Richardson, Keenan, Migliavacca, Ryu, Sonnentag, & Toomey, 2013; Keenan et al., 2014),  
94 whereas atmospheric inversion data and vegetation photosynthesis model indicated a dominant  
95 role of the maximal carbon uptake rate (Fu, Dong, Zhou, Stoy, & Niu, 2017; Zhou et al., 2017).  
96 However, the relative importance of these phenological and physiological indicators for the  
97 spatially varying NEP remains unclear.

98 In this study, we first explored the changes in NEP and IAV<sub>NEP</sub> at the global scale based  
99 on data from a widely-used machine-learning-derived product (i.e., FLUXCOM). To address  
100 the local indicators for spatially varying NEP, we decomposed annual NEP into  $U$  and  $R$ . Then,  
101 we examined the relationship of  $NEP \propto \frac{U}{R}$  based on the observations at 72 eddy covariance  
102 towers which has >5 years measurements in the FLUXNET2015 Dataset (Jung et al., 2017). In  
103 addition, we used the observations to evaluate the spatial variations of NEP and IAV<sub>NEP</sub> in the  
104 FLUXCOM database and a process-based model (CLM4.5) (Oleson et al., 2013). The major  
105 aim of this study is to explore whether there are useful local indicators for the spatially varying  
106 NEP and IAV<sub>NEP</sub> in terrestrial ecosystems.

## 107 **2. Materials and Methods**

### 108 **2.1 Datasets**

109 Daily NEP observations of eddy covariance sites were obtained from the FLUXNET2015 Tier  
110 1 dataset (<http://fluxnet.fluxdata.org/data/fluxnet2015-dataset/>). The FLUXNET2015 dataset



111 provides half-hourly data of carbon, water and energy fluxes at over 210 sites that are  
112 standardized and gap-filled (Pastorello et al., 2017). However, time series of most sites are still  
113 too short for the analysis of inter-annual variation in NEP. So only the sites that provided the  
114 availability of eddy covariance flux measurements for at least 5 years are selected. This leads  
115 to a global dataset of 72 sites with different biomes across different climatic regions. Based on  
116 the biome classification from the International Geosphere-Biosphere Programme (IGBP)  
117 provided for the FLUXNET2015 sites, the selected sites include 35 forests (FOR), 15  
118 grasslands (GRA), 11 croplands (CRO), 4 wetlands (WET), 2 shrublands (SHR) and 5  
119 savannas (SAV) (Fig. S1 and Table S1). The stand age information of forest sites is the average  
120 tree age of the stand, and was obtained from the Biological Ancillary Disturbance and  
121 Metadata (BAMD) of the FLUXNET dataset (Musavi, et al., 2017).

122 The FLUXCOM dataset presents an upscaling of carbon flux estimates from 224 flux  
123 tower sites based on multiple machine learning algorithms and satellite data (Jung et al., 2017).  
124 Meteorological measurements from CRUNCEPv6 and a series of remotely sensed datasets  
125 were used as input. For this study, we downloaded the NEP product from the Data Portal of the  
126 Max Planck Institute for Biochemistry (<https://www.bgc-jena.mpg.de>). Daily outputs from  
127 FLUXCOM for the period 1980-2013 were used to map the spatial variation in terrestrial NEP  
128 and calculate the local indicators for the spatially varying NEP at the same locations of the flux  
129 tower sites.

130 Daily NEP simulations from Community Land Model version 4.5 (CLM4.5) were also  
131 used to calculate the local indicators for the spatially varying NEP at the corresponding flux  
132 tower sites. We ran the CLM4.5 model from 1990 to 2010 with a spatial resolution of 1° to  
133 match the available FLUXCOM dataset. Here, NEP was derived as the difference between  
134 GPP and TER, and TER was calculated as the sum of simulated autotrophic and heterotrophic  
135 respiration. The daily outputs from CLM4.5 were used to calculate the local indicators for the  
136 spatially varying NEP at the same locations of the flux tower sites.

## 137 **2.2 Decomposition of NEP and the calculations for its local indicators**



138 The annual NEP of a given ecosystem can be defined numerically as the difference between  
139 the CO<sub>2</sub> uptake and release. As illustrated in Figure 2b:

$$140 \quad \quad \quad NEP = U - R \quad \quad \quad (1)$$

141 where the total CO<sub>2</sub> uptake flux ( $U$ ) and the total CO<sub>2</sub> release flux ( $R$ ) can be further  
142 decomposed as:

$$143 \quad \quad \quad U = \bar{U} \times CUP \quad \quad \quad (2)$$

$$144 \quad \quad \quad R = \bar{R} \times CRP \quad \quad \quad (3)$$

145 where the  $\bar{U}$  (g C m<sup>-2</sup> d<sup>-1</sup>) is the mean daily CO<sub>2</sub> uptake over  $CUP$  and  $\bar{R}$  (g C m<sup>-2</sup> d<sup>-1</sup>)  
146 represents the mean daily CO<sub>2</sub> release over  $CRP$ . The calculations of these direct indicators are  
147 as follows:

$$148 \quad \quad \quad U = \sum_{i=1}^m NEP_i \quad (NEP_i > 0; CUP = m) \quad \quad \quad (4)$$

$$149 \quad \quad \quad R = \sum_{i=1}^n NEP_i \quad (NEP_i < 0; CRP = n) \quad \quad \quad (5)$$

150 where  $NEP_i$  refers to the daily NEP (g C m<sup>-2</sup> d<sup>-1</sup>) in the  $i$ th day. Because many studies have  
151 reported that the vegetation CO<sub>2</sub> uptake during the growing season and the non-growing soil  
152 respiration are tightly correlated (Luo, & Zhou, 2006; Xia, Chen, Piao, Ciais, Luo, & Wan,  
153 2014; Zhao, Peichl, Öquist, & Nilsson, 2016), we further tested the relationship between  
154 annual NEP and the ratio of  $\frac{U}{R}$  (i.e.,  $NEP \propto \frac{U}{R}$ ). Then we found that annual NEP was closely  
155 related with the ratio of  $\frac{U}{R}$  (Figure S2). Therefore, NEP in any year of any given ecosystem  
156 can be expressed as:

$$157 \quad \quad \quad NEP = \beta \cdot \ln\left(\frac{U}{R}\right) \quad \quad \quad (6)$$

158 where the parameter  $\beta$  represents the slope of the linear relationship of  $NEP \propto \ln\left(\frac{U}{R}\right)$ . Based  
159 on the definitions of  $U$  and  $R$ , the ratio  $\frac{U}{R}$  can be further written as:

$$160 \quad \quad \quad \frac{U}{R} = \frac{\bar{U}}{\bar{R}} \cdot \frac{CUP}{CRP} \quad \quad \quad (7)$$



161        These components of NEP contain both photosynthesis and respiration flux, which  
162        directly indicate the net CO<sub>2</sub> exchange of an ecosystem. Ecologically, the ratio of  $\frac{\bar{U}}{R}$  reflects  
163        the relative physiological difference between ecosystem CO<sub>2</sub> uptake and release strength,  
164        while the ratio of  $\frac{CUP}{CRP}$  is an indicator of net ecosystem CO<sub>2</sub> exchange phenology.  
165        Environmental changes may regulate these ecological processes and ultimately affect the  
166        ecosystem NEP. The slope  $\beta$  indicates the response sensitivity of NEP to the changes in  
167        phenology and physiological processes. All of  $\beta$ ,  $\frac{CUP}{CRP}$  and  $\frac{\bar{U}}{R}$  were then calculated from the  
168        selected eddy covariance sites and the corresponding pixels of these sites in models. These  
169        derived indicators from eddy covariance sites were then used to benchmark the results  
170        extracted from the same locations in models.

#### 171    2.4 Calculation of the relative contributions

172        To further identify the relative contributions of  $\frac{\bar{U}}{R}$  and  $\frac{CUP}{CRP}$  in driving the spatiotemporal  
173        variations in the local indicator  $\frac{U}{R}$ , we linearized the equation (7) as

$$174 \quad \log\left(\frac{U}{R}\right) = \log\left(\frac{\bar{U}}{R}\right) + \log\left(\frac{CUP}{CRP}\right) \quad (8)$$

175        Then we used a relative importance analysis method to quantify the relative contributions  
176        of each ratio to the spatiotemporal variations in  $\frac{U}{R}$ . The algorithm was performed with the  
177        “ralaimpo” package in R (R Development Core Team, 2011). The “ralaimpo” package is based  
178        on variance decomposition for multiple linear regression models. We chose the most  
179        commonly used method named “Lindeman-Merenda-Gold (LMG)” (Grömping, 2007) from  
180        the methods provided by the “ralaimpo” package. This method allows us to quantify the  
181        contributions of explanatory variables in a multiple linear regression model. In each site, we  
182        calculated the contributions of  $\frac{\bar{U}}{R}$  and  $\frac{CUP}{CRP}$  in explaining inter-annual variation in  $\frac{U}{R}$ . Across  
183        the 72 FLUXNET sites, we quantified the relative importance of  $\frac{\bar{U}}{R}$  and  $\frac{CUP}{CRP}$  to cross-site  
184        changes in  $\frac{U}{R}$ .

### 185    3. Results



### 186 3.1 Spatial variability in terrestrial NEP

187 Based on the FLUXCOM product, a large spatial variation in terrestrial NEP and  $IAV_{NEP}$   
188 existed over 1980-2013. The tropical forests were typically large carbon sinks accompanied by  
189 considerable interannual variability. On the contrary, the boreal tundra ecosystems were stable  
190 carbon sinks and the shrublands in the Southern Hemisphere were variable carbon sources (Fig.  
191 1a). This remarkable spatial difference in terrestrial NEP was particularly obvious from  
192 eddy-flux measurements (Fig. S1), and the global average IAV of NEP ( $175 \pm 111 \text{ g C m}^{-2} \text{ yr}^{-1}$ )  
193 was large relative to global annual mean NEP ( $216 \pm 234 \text{ g C m}^{-2} \text{ yr}^{-1}$ ). These spatial patterns  
194 were also supported by the model outputs (Jung et al., 2017) and atmospheric inversion product  
195 (Marcolla, Rödenbeck, & Cescatti, 2017).

196 More importantly, we found that the variations of NEP and  $IAV_{NEP}$  were spatially  
197 asynchronous. Along the latitudinal gradients, terrestrial NEP peaked at equatorial regions,  
198 whereas the highest  $IAV_{NEP}$  existed in semiarid regions near  $37^\circ \text{ S}$  (Fig. 1b). The demonstrated  
199 spatial asynchrony further revealed the necessary to identify local indicators for the spatially  
200 varying NEP and  $IAV_{NEP}$ , separately.

### 201 3.2 Local indicators for spatially varying NEP

202 To find local indicators for the spatially varying NEP in terrestrial ecosystems, we first tested  
203 the relationship between NEP and the  $\frac{U}{R}$  ratio across the 72 flux-tower sites. We found robust  
204 logarithmic correlation between annual NEP and  $\frac{U}{R}$  at all sites (Fig. 2a; Fig. S2), with  $\sim 90\%$   
205 of  $R^2$  falling within a range from 0.7 to 1 (Fig. 2c). Across the 72 flux-tower sites, the spatial  
206 changes in mean annual NEP were significantly correlated to  $\ln\left(\frac{U}{R}\right)$  ( $R^2 = 0.65$ ,  $P < 0.01$ )  
207 (Fig. 3a). This finding suggests that the mean annual ratio  $\ln\left(\frac{U}{R}\right)$  is a good indicator for NEP  
208 and its spatial variation. By contrast, the spatial variation of  $IAV_{NEP}$  was well explained by the  
209 slope (i.e.,  $\beta$ ) of the temporal correlation between NEP and  $\ln\left(\frac{U}{R}\right)$  at each site ( $R^2 = 0.39$ ,  $P <$   
210  $0.01$ ; Fig. 3b) rather than  $\ln\left(\frac{U}{R}\right)$  (Fig. S3). The wide range of ratio  $\beta$  reveals a large  
211 divergence of NEP sensitivity across biomes, ranging from  $121 \pm 118 \text{ g C m}^{-2} \text{ yr}^{-1}$  in shrubland  
212 to  $473 \pm 112 \text{ g C m}^{-2} \text{ yr}^{-1}$  in cropland.



213 The decomposition of indicator  $\frac{U}{R}$  into  $\frac{\bar{U}}{\bar{R}}$  and  $\frac{CUP}{CRP}$  allowed us to quantify the relative  
214 importance of these two ratios in driving  $\frac{U}{R}$  variability. The linear regression and relative  
215 importance analysis showed a more important role of  $\frac{CUP}{CRP}$  (81%) than  $\frac{\bar{U}}{\bar{R}}$  (19%) in explaining  
216 the cross-site variation of  $\frac{U}{R}$  (Fig. 4). Therefore, the spatial distribution of mean annual NEP  
217 was mostly driven by the phenological rather than physiological changes.

### 218 3.3 Simulated spatial variations in NEP by models

219 We further used these two simple indicators (i.e.,  $\frac{U}{R}$  and  $\beta$ ) to evaluate the simulated spatial  
220 variations of NEP by the machine-learning approach (i.e., FLUXCOM) and a widely-used  
221 process-based model (i.e., CLM4.5). We found that both of FLUXCOM and CLM4.5  
222 underestimated the spatial variation of mean annual NEP and  $IAV_{NEP}$  (Fig. 5a). The low spatial  
223 variation of mean annual NEP in FLUXCOM and CLM4.5 could be inferred from their more  
224 converging  $\ln\left(\frac{U}{R}\right)$  than flux-tower measurements (Fig. 5b). The underestimated variation of  
225  $IAV_{NEP}$  in these modeling results was also clearly shown by the smaller  $\beta$  values (268.22,  
226 126.00 and 145.08 for FLUXNET, FLUXCOM and CLM4.5, respectively) (Fig. 5b).

## 227 4. Discussion

### 228 4.1 New perspective for locating the major and sustainable land C sinks

229 Large spatial differences of mean annual NEP and  $IAV_{NEP}$  have been well-documented in  
230 previous studies (Jung et al., 2017; Marcolla, Rödenbeck, & Cescatti, 2017; Fu et al., 2019).  
231 Here we provide a new perspective for quantifying the spatially varying NEP by tracing  
232 annual NEP into several local indicators. Therefore, these traceable indicators could provide  
233 useful constraints for predicting annual NEP, especially in areas without eddy-covariance  
234 towers.

235 Typically, the C sink capacity and its stability of a specific ecosystem are characterized  
236 separately (Keenan et al., 2014; Ahlstrom et al., 2015; Jung et al., 2017). Here we integrated  
237 NEP into two simple indicators that could directly locate the major and sustainable land C sink.  
238 Among biomes, forests and croplands had the largest  $\ln\left(\frac{U}{R}\right)$  and  $\beta$ , indicating the strongest



239 and the most unstable C sink in forests and croplands, respectively. The highest  $\beta$  in croplands  
240 implies that the rapid global expansion of cropland may enlarge the  $I_{AVNEP}$  on the land. In fact,  
241 the cropland expansion has been confirmed as one important driver of the recent increasing  
242 global vegetation growth peak (Huang et al., 2018) and atmospheric  $CO_2$  seasonal amplitude  
243 (Gary et al., 2014; Zeng et al., 2014).

#### 244 **4.2 Phenology-dominant spatial distribution of mean annual NEP**

245 Recent studies have demonstrated that the spatiotemporal variations in terrestrial gross  
246 primary productivity are jointly controlled by plant phenology and physiology (Xia et al., 2015;  
247 Zhou et al., 2016). Here we demonstrated the dominant role of the phenology indicator  $\frac{CUP}{CRP}$  in  
248 driving the spatial difference of  $\frac{U}{R}$  and therefore the mean annual NEP. The reported low  
249 correlation between  $\frac{U}{R}$  and the physiological indicator  $\frac{U}{R}$  could partly be attributed to the  
250 convergence of  $\frac{\bar{U}}{\bar{R}}$  across FLUXNET sites (Fig. S4). The convergent  $\frac{\bar{U}}{\bar{R}}$  across sites was first  
251 discovered by Churkina *et al.* (2005) as  $2.73 \pm 1.08$  across 28 sites, which included DBF, EBF  
252 and crop/grass. In this study, we found the  $\frac{\bar{U}}{\bar{R}}$  across the 72 sites is  $2.71 \pm 1.61$ , which  
253 validates the discovery by Churkina *et al.* However, the  $\frac{\bar{U}}{\bar{R}}$  varied among biomes ( $2.86 \pm 1.56$   
254 for forest,  $2.16 \pm 1.14$  for grassland,  $3.47 \pm 1.98$  for cropland,  $2.89 \pm 1.47$  for wetland,  $1.89 \pm$   
255  $1.10$  for shrub,  $1.83 \pm 0.88$  for savanna). This spatial convergence of  $\frac{\bar{U}}{\bar{R}}$  at the ecosystem level  
256 provides important constraints for global models that simulate various physiological processes  
257 (Peng et al., 2015; Xia et al., 2017). These findings imply that the phenology changes will  
258 greatly affect the locations of the terrestrial carbon sink by modifying the length of carbon  
259 uptake period (Richardson, Keenan, Migliavacca, Ryu, Sonnentag, & Toomey, 2013; Keenan  
260 et al., 2014).

#### 261 **4.3 The underestimated spatial variations of NEP in models**

262 This study showed that the considerable spatial variations in mean annual NEP and  $I_{AVNEP}$   
263 were both underestimated by the machine-learning-based and process-based global models,  
264 which could also be inferred from their local indicators. The low variations of  $\frac{U}{R}$  ratio in the



265 two modeling approaches could be largely due to their simple representations of the diverse  
266 terrestrial plant communities into a few plant functional types with parameterized properties  
267 (Sakschewski et al., 2015). The ignorance of year-to-year vegetation dynamic could lead to the  
268 smaller  $\beta$  by allowing for only limited variations of phenological and physiological responses  
269 to environmental changes (Reichstein, Bahn, Mahecha, Kattge, & Baldocchi, 2014; Kunstler  
270 et al., 2016). Although the magnitude of  $I_{AV_{NEP}}$  depends on the spatial resolution (Marcolla,  
271 Rödenbeck, & Cescatti, 2017), we recommend future model benchmarking analyses to use not  
272 only the machine-learning-based data product (Bonan et al., 2018) but also the site-level  
273 measurements or indicators (i.e.,  $\ln\left(\frac{U}{R}\right)$  and  $\beta$ ).

#### 274 4.4 Conclusions and further implications

275 In summary, the findings in this study have some important implications for understanding the  
276 variation of NEP on the land. First, forest ecosystems have the largest annual NEP due to the  
277 largest  $\ln\left(\frac{U}{R}\right)$  while croplands show the highest  $I_{AV_{NEP}}$  because of the highest  $\beta$ . Second, the  
278 spatial convergence of  $\frac{\bar{U}}{\bar{R}}$  suggests a tight linkage between plant growth and the non-growing  
279 season soil microbial activities (Xia, Chen, Piao, Ciais, Luo, & Wan, 2014; Zhao, Peichl,  
280 Öquist, & Nilsson, 2016). However, it remains unclear whether the inter-biome variation in  $\frac{U}{R}$   
281 is due to different plant-microbe interactions between biomes. Third, the within-site  
282 convergent but spatially varying  $\beta$  needs better understanding. Previous studies have shown  
283 that a rising standard deviation of ecosystem functions could indicate an impending ecological  
284 state transition (Carpenter, & Brock, 2006; Scheffer et al., 2009). Thus, a sudden shift of the  
285  $\beta$ -value may be an important early-warning signal for the critical transition of  $I_{AV_{NEP}}$  of an  
286 ecosystem.

287 In addition, considering the limited eddy-covariance sites with long-term observations,  
288 these findings need further validation once the longer time-series of measurements from more  
289 sites and vegetation types become available. Overall, this study highlights the asynchronous  
290 changes in NEP and  $I_{AV_{NEP}}$  over space on the land, and provides the  $\frac{U}{R}$  ratio and  $\beta$  as two  
291 simple local indicators for their spatial variations. These indicators could be helpful for



292 locating the persistent terrestrial C sinks in where the  $\ln\left(\frac{U}{R}\right)$  ratio is high but the  $\beta$  is low.  
293 Their estimates based on observations are also valuable for benchmarking and improving the  
294 simulation of land-atmospheric C exchanges in Earth system models.

### 295 **Acknowledgements**

296 This work was financially supported by the National Key R&D Program of China  
297 (2017YFA0604600), National Natural Science Foundation of China (31722009, 41630528)  
298 and National 1000 Young Talents Program of China. This work used eddy covariance dataset  
299 acquired and shared by the FLUXNET community, including these networks: AmeriFlux,  
300 AfriFlux, AsiaFlux, CarboAfrica, CarboEuropeIP, CarboItaly, CarboMont, ChinaFlux,  
301 Fluxnet-Canada, GreenGrass, ICOS, KoFlux, LBA, NECC, OzFlux-TERN, TCOS-Siberia,  
302 and USCCC. The ERA-Interim reanalysis data are provided by ECMWF and processed by  
303 LSCE. The FLUXNET eddy covariance data processing and harmonization was carried out by  
304 the European Fluxes Database Cluster, AmeriFlux Management Project, and Fluxdata project  
305 of FLUXNET, with the support of CDIAC and ICOS Ecosystem Thematic Center, and the  
306 OzFlux, ChinaFlux and AsiaFlux offices.

307 *Data availability statement.* Eddy flux data are available at  
308 <http://fluxnet.fluxdata.org/data/fluxnet2015-dataset/>; the data supporting the findings of this  
309 study are available within the article and the Supplementary Information.

310 *Author contribution.* E. Cui and J. Xia devised and conducted the analysis. Y. Luo, S. Niu, Y.  
311 Wang and C. Bian provided critical feedback on the method and results. All authors  
312 contributed to discussion of results and writing the paper.

313 *Competing interests.* The authors declare that there is no conflict of interest.



314 **FIGURES**

315 **Figure 1** Locations of carbon sinks (mean annual NEP) and their stability ( $IAV_{NEP}$ ) on the land.

316 a, Spatial patterns of mean annual NEP and  $IAV_{NEP}$ . b, Latitudinal patterns of mean annual  
317 NEP and  $IAV_{NEP}$ .

318 **Figure 2** Relationship between annual NEP and  $\frac{U}{R}$  for 72 FLUXNET sites (of the form

319  $NEP = \beta \cdot \ln\left(\frac{U}{R}\right)$ ). a, Dependence of annual NEP on the ratio between total  $CO_2$  exchanges

320 during net uptake ( $U$ ) and release ( $R$ ) periods (i.e.,  $\frac{U}{R}$ ). Each line represents one flux site with

321 at least 5 years of observations. b, Conceptual figure for the decomposition framework

322 introduced in this study. Annual NEP can be quantitatively decomposed into the following

323 indicators:  $NEP = U - R$ . c, Distribution of the explanation of  $\frac{U}{R}$  on temporal variability of

324 NEP ( $R^2$ ) for FLUXNET sites.

325 **Figure 3** Contributions of the two indicators in explaining the spatial patterns of mean annual

326 NEP and  $IAV_{NEP}$ . a, The relationship between annual mean NEP and  $\ln\left(\frac{U}{R}\right)$  across

327 FLUXNET sites ( $R^2 = 0.65$ ,  $P < 0.01$ ). The insets show the variation of  $\ln\left(\frac{U}{R}\right)$  for different

328 terrestrial biomes. b, The explanation of  $\beta$  on  $IAV_{NEP}$  ( $R^2 = 0.39$ ,  $P < 0.01$ ). The insets show

329 the distribution of parameter  $\beta$  for different terrestrial biomes. The number of site-years at

330 each site is indicated with the size of the point.

331 **Figure 4** The linear regression between  $\frac{U}{R}$  with  $\frac{CUP}{CRP}$  ( $R^2 = 0.71$ ,  $P < 0.01$ ) and  $\frac{\bar{U}}{R}$  ( $R^2 = 0.09$ ,

332  $P < 0.01$ ) across sites. The insets show the relative contributions of each indicator to the

333 spatial variation of  $\frac{U}{R}$ . The number of site-years at each site is indicated with the size of the

334 point.

335 **Figure 5** Representations of the spatially varying NEP and its local indicators in FLUXCOM

336 product and the Community Land Model (CLM4.5). a, The variation of mean annual NEP and

337  $IAV_{NEP}$  derives from FLUXNET, FLUXCOM and CLM4.5. Variation in mean annual NEP:

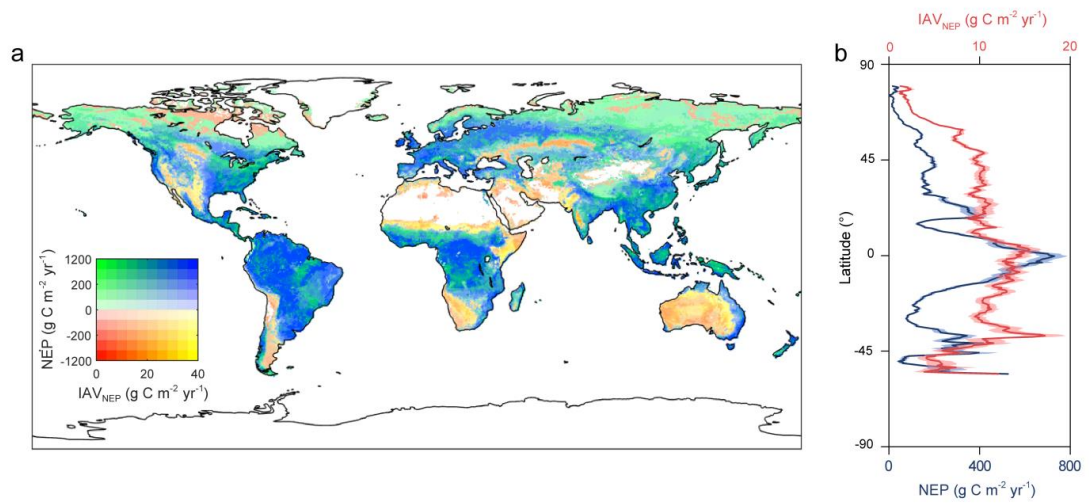
338 the standard deviation of mean annual NEP across sites; Variation in  $IAV_{NEP}$ : the standard

339 deviation of  $IAV_{NEP}$  across sites. b, Representations of the local indicators for NEP in

340 FLUXNET, FLUXCOM and CLM4.5. The corresponding distributions of  $\ln\left(\frac{U}{R}\right)$  and  $\beta$  are



341 shown at the top and right. Significance of the relationship between annual NEP and  $\ln\left(\frac{U}{R}\right)$   
342 for each site is indicated by the circle: closed circles:  $P < 0.05$ ; open circles:  $P > 0.05$ . Note that  
343 the modeled results are from the pixels extracted from the same locations of the flux tower  
344 sites.  
345



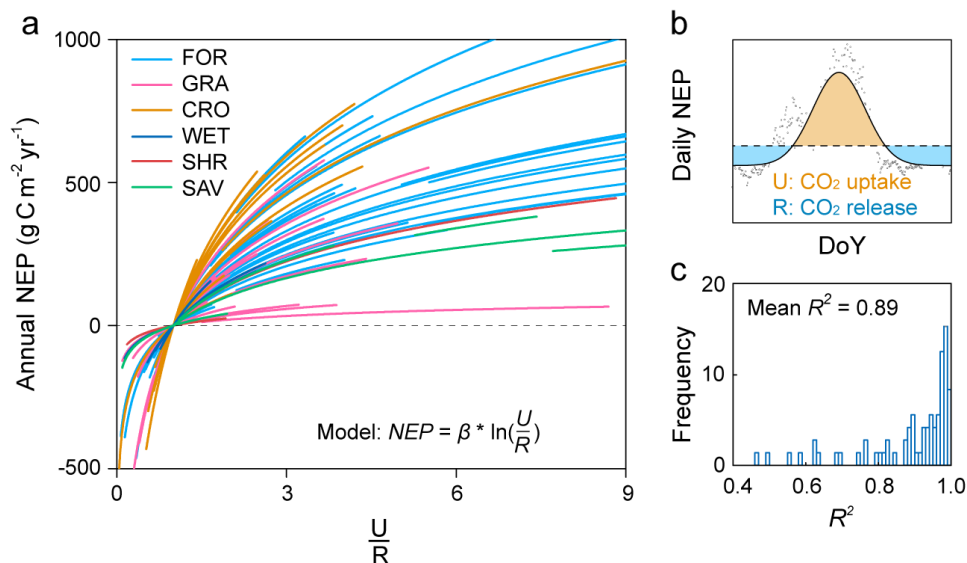
346

347 **Figure 1** Locations of carbon sinks (mean annual NEP) and their stability (IAV<sub>NEP</sub>) on the land.

348 **a**, Spatial patterns of mean annual NEP and IAV<sub>NEP</sub>. **b**, Latitudinal patterns of mean annual

349 NEP and IAV<sub>NEP</sub>.

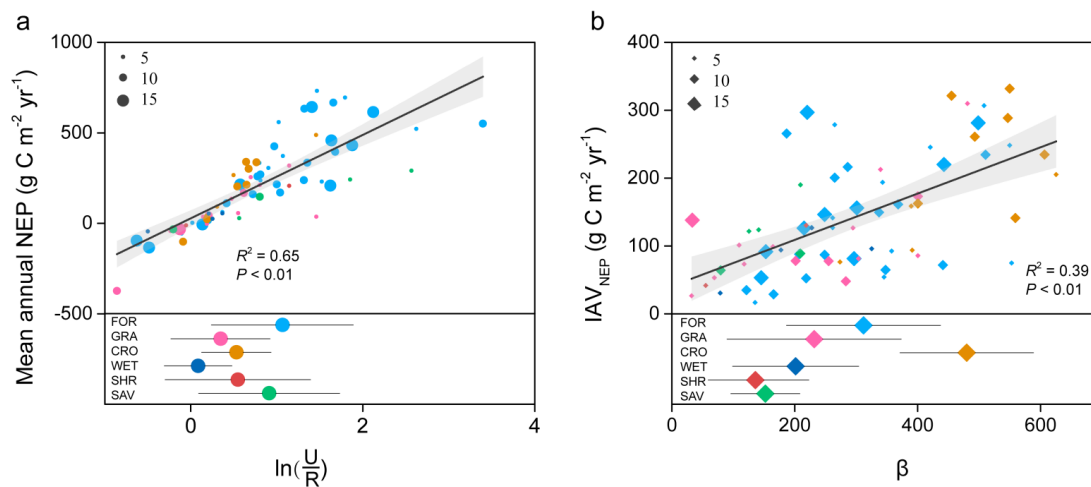
350



351

352 **Figure 2** Relationship between annual NEP and  $\frac{U}{R}$  for 72 FLUXNET sites (of the form  
 353  $NEP = \beta \cdot \ln\left(\frac{U}{R}\right)$ ). **a**, Dependence of annual NEP on the ratio between total CO<sub>2</sub> exchanges  
 354 during net uptake ( $U$ ) and release ( $R$ ) periods (i.e.,  $\frac{U}{R}$ ). Each line represents one flux site with  
 355 at least 5 years of data. **b**, Conceptual figure for the decomposition framework introduced in  
 356 this study. Annual NEP can be quantitatively decomposed into the following indicators:  
 357  $NEP = U - R$ . **c**, Distribution of the explanation of  $\frac{U}{R}$  on temporal variability of FLUXNET  
 358 NEP ( $R^2$ ) for FLUXNET sites.

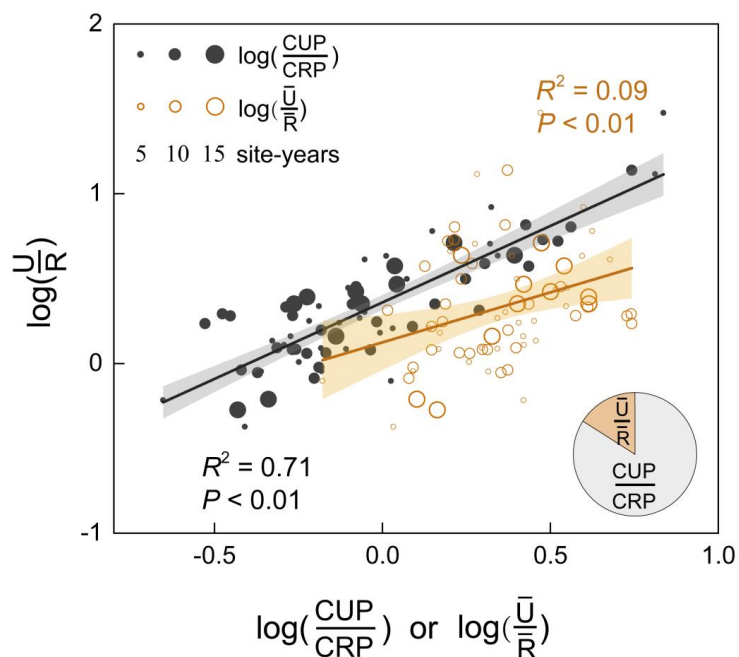
359



360

361 **Figure 3** Contributions of the two indicators in explaining the spatial patterns of mean annual  
362 NEP and IAV<sub>NEP</sub>. **a**, The relationship between annual mean NEP and  $\ln\left(\frac{U}{R}\right)$  across  
363 FLUXNET sites ( $R^2 = 0.65$ ,  $P < 0.01$ ). The insets show the variation of  $\ln\left(\frac{U}{R}\right)$  for different  
364 terrestrial biomes. **b**, The explanation of  $\beta$  on IAV<sub>NEP</sub> ( $R^2 = 0.39$ ,  $P < 0.01$ ). The insets show  
365 the distribution of parameter  $\beta$  for different terrestrial biomes. The number of site-years at  
366 each site is indicated with the size of the point.

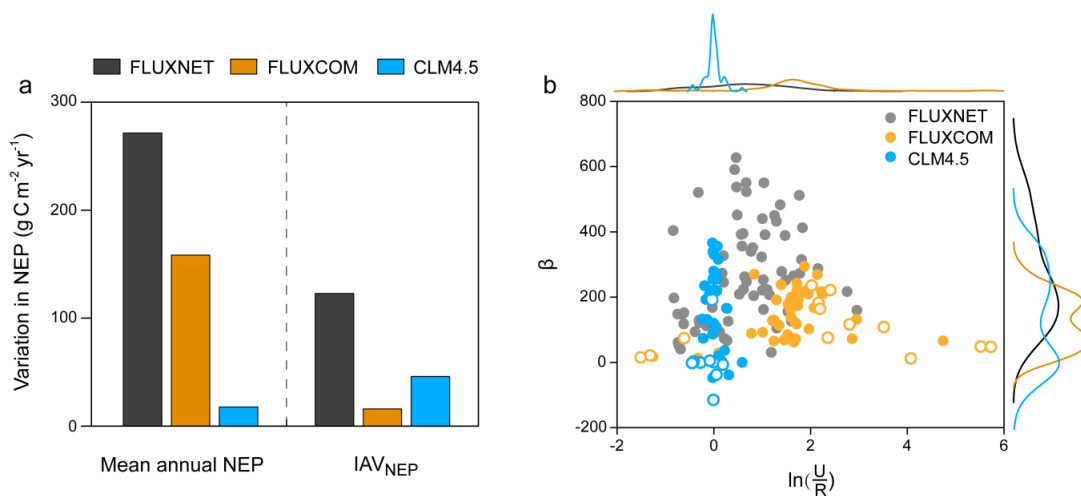
367



368

369 **Figure 4** The linear regression between  $\frac{U}{R}$  with  $\frac{CUP}{CRP}$  ( $R^2 = 0.71$ ,  $P < 0.01$ ) and  $\frac{\bar{U}}{\bar{R}}$  ( $R^2 = 0.09$ ,  
370  $P < 0.01$ ) across sites. The insets show the relative contributions of each indicator to the  
371 spatial variation of  $\frac{U}{R}$ . The number of site-years at each site is indicated with the size of the  
372 point.

373



374

375 **Figure 5** Representations of the spatially varying NEP and its local indicators in FLUXCOM  
376 product and the Community Land Model (CLM4.5). **a**, The variation of mean annual NEP and  
377 IAV<sub>NEP</sub> derives from FLUXNET, FLUXCOM and CLM4.5. Variation in mean annual NEP:  
378 the standard deviation of mean annual NEP across sites; Variation in IAV<sub>NEP</sub>: the standard  
379 deviation of IAV<sub>NEP</sub> across sites. **b**, Representations of the local indicators for NEP in  
380 FLUXNET, FLUXCOM and CLM4.5. The corresponding distributions of  $\ln\left(\frac{U}{R}\right)$  and  $\beta$  are  
381 shown at the top and right. Significance of the relationship between annual NEP and  
382  $\ln\left(\frac{U}{R}\right)$  for each site is indicated by the circle: closed circles:  $P < 0.05$ ; open circles:  $P > 0.05$ .  
383 Note that the modeled results are from the pixels extracted from the same locations of the flux  
384 tower sites.

385

386



## 387 References

- 388 Ahlström, A., Raupach, M. R., Schurgers, G., Smith, B., Arneth, A., Jung, M., Reichstein, M.,  
389 Canadell, J. G., Friedlingstein, P., Jain, A. K., Kato, E., Poulter, B., Sitch, S., Stocker, B.  
390 D., Viovy, N., Wang, Y., Wiltshire, A., Zaehle, S., and Zeng, N.: The dominant role of  
391 semi-arid ecosystems in the trend and variability of the land CO<sub>2</sub> sink. *Science*, 348,  
392 895-899, 2015.
- 393 Baldocchi, D., Chu, H., and Reichstein, M.: Inter-annual variability of net and gross ecosystem  
394 carbon fluxes: A review. *Agric. For. Meteorol.*, 249, 520-533, 2018.
- 395 Baldocchi, D., Sturtevant, C., and Contributors, F.: Does day and night sampling reduce  
396 spurious correlation between canopy photosynthesis and ecosystem respiration? *Agric.*  
397 *For. Meteorol.*, 207, 117-126, 2015.
- 398 Biederman, J. A., Scott, R. L., Goulden, M. L., Vargas, R., Litvak, M. E., Kolb, T. E., Yopez, E.  
399 A., Oechel, W. C., Blanken, P. D., Bell, T. W., Garatuza-Payan, J., Maurer, . E., Dore, S.,  
400 and Burns, S. P.: Terrestrial carbon balance in a drier world: the effects of water  
401 availability in southwestern North America. *Glob. Change Biol.*, 22, 1867-1879, 2016.
- 402 Bonan, G. B., Patton, E. G., Harman, I. N., Oleson, K. W., Finnigan, J. J., Lu, Y., and  
403 Burakowski, E. A.: Modeling canopy-induced turbulence in the Earth system: a unified  
404 parameterization of turbulent exchange within plant canopies and the roughness sublayer  
405 (CLM-ml v0). *Geosci. Model Dev.*, 11, 1467-1496, 2018.
- 406 Carpenter, S. R., and Brock, W. A.: Rising variance: a leading indicator of ecological transition.  
407 *Ecol. Lett.*, 9, 311-318, 2006.
- 408 Churkina, G., Schimel, D., Braswell, B. H., and Xiao, X.: Spatial analysis of growing season  
409 length control over net ecosystem exchange. *Glob. Change Biol.*, 11, 1777-1787, 2005.
- 410 Ciais, P., Tan, J., Wang, X., Roedenbeck, C., Chevallier, F., Piao, S. L., Moriarty, R., Broquet,  
411 G., Le Quéré, C., Canadell, J. G., Peng, S., Poulter, B., Liu Z., and Tans, P.: Five decades  
412 of northern land carbon uptake revealed by the interhemispheric CO<sub>2</sub> gradient. *Nature*,  
413 568, 221-225, 2019.
- 414 Fu, Z., Dong, J., Zhou, Y., Stoy, P. C., and Niu, S.: Long term trend and interannual variability  
415 of land carbon uptake-the attribution and processes. *Environ. Res. Lett.*, 12, 014018,  
416 2017.
- 417 Fu, Z., Stoy, P. C., Poulter, B., Gerken, T., Zhang, Z., Wakbulcho, G., and Niu, S.: Maximum  
418 carbon uptake rate dominates the interannual variability of global net ecosystem  
419 exchange. *Glob. Change Biol.*, 25, 3381-3394, 2019.
- 420 Gilmanov, T. G., Tieszen, L. L., Wylie, B. K., Flanagan, L. B., Frank, A. B., Haferkamp, M. R.,  
421 Meyers, T. P., and Morgan, J. A.: Integration of CO<sub>2</sub> flux and remotely-sensed data for  
422 primary production and ecosystem respiration analyses in the Northern Great Plains:  
423 Potential for quantitative spatial extrapolation. *Global Ecol. Biogeogr.*, 14, 271-292,  
424 2005.



- 425 Gray, J. M., Frolking, S., Kort, E. A., Ray, D. K., Kucharik, C. J., Ramankutty, N., and Friedl,  
426 M. A.: Direct human influence on atmospheric CO<sub>2</sub> seasonality from increased cropland  
427 productivity. *Nature*, 515, 398-401, 2014.
- 428 Grömping, U.: Estimators of relative importance in linear regression based on variance  
429 decomposition. *Am. Stat.*, 61, 139-147, 2007.
- 430 Huang, K., Xia, J., Wang, Y., Ahlström, A., Chen, J., Cook, R. B., Cui, E., Fang, Y., Fisher, J.  
431 B., Huntzinger, D. N., Li, Z., Michalak, A. M., Qiao, Y., Schaefer, K., Schwalm, C., Wang,  
432 J., Wei, Y., Xu, X., Yan, L., Bian C., and Luo, Y.: Enhanced peak growth of global  
433 vegetation and its key mechanisms. *Nat. Ecol. Evol.*, 2, 1897-1905, 2018.
- 434 Jung, M., Reichstein, M., Schwalm, C. R., Huntingford, C., Sitch, S., Ahlström, A., Arneeth, A.,  
435 Camps-Valls, G., Ciais, P., Friedlingstein, P., Gans, F., Ichii, K., Jain, A. K., Kato, E.,  
436 Papale, D., Poulter, B., Raduly, B., Rödenbeck, C., Tramontana, G., Viovy, N., Wang, Y.,  
437 Weber, U., Zaehle S., and Zeng, N.: Compensatory water effects link yearly global land  
438 CO<sub>2</sub> sink changes to temperature. *Nature*, 541, 516-520, 2017.
- 439 Keenan, T. F., Gray, J., Friedl, M. A., Toomey, M., Bohrer, G., Hollinger, D. Y., Munger, J. W.,  
440 O’Keefe, J., Schmid, H. P., Wing, I. S., Yang, B., and Richardson, A. D.: Net carbon  
441 uptake has increased through warming-induced changes in temperate forest phenology.  
442 *Nat. Clim. Change*, 4, 598-604, 2014.
- 443 Kunstler, G., Falster, D., Coomes, D. A., Hui, F., Kooyman, R. M., Laughlin, D. C., Poorter, L.,  
444 Vanderwel, M., Vieilledent, G., Wright, S. J., Aiba, M., Baraloto, C., Caspersen, J.,  
445 Cornelissen, J. H. C., Gourlet-Fleury, S., Hanewinkel, M., Herault, B., Kattge, J.,  
446 Kurokawa, H., Onoda, Y., Peñuelas, J., Poorter, H., Uriarte, M., Richardson, S.,  
447 Ruiz-Benito, P., Sun, I., Ståhl, G., Swenson, N. G., Thompson, J., Westerlund, B., Wirth,  
448 C., Zavalá, M. A., Zeng, H., Zimmerman, J. K., Zimmermann N. E., and Westoby, M.:  
449 Plant functional traits have globally consistent effects on competition. *Nature*, 529,  
450 204-207, 2016.
- 451 Le Quéré, C., Andrew, R. M., Friedlingstein, P., Sitch, S., Hauck, J., Pongratz, J., Pickers, P. A.,  
452 Korsbakken, J. I., Peters, G. P., Canadell, J. G., Arneeth, A., Arora, V. K., Barbero, L.,  
453 Bastos, A., Bopp, L., Chevallier, F., Chini, L. P., Ciais, P., Doney, S. C., Gkritzalis, T.,  
454 Goll, D. S., Harris, I., Haverd, V., Hoffman, F. M., Hoppema, M., Houghton, R. A., Hurtt,  
455 G., Ilyina, T., Jain, A. K., Johannessen, T., Jones, C. D., Kato, E., Keeling, R. F.,  
456 Goldewijk, K. K., Landschützer, P., Lefèvre, N., Lienert, S., Liu, Z., Lombardozzi, D.,  
457 Metzl, N., Munro, D. R., Nabel, J. E. M. S., Nakaoka, S., Neill, C., Olsen, A., Ono, T.,  
458 Patra, P., Peregon, A., Peters, W., Peylin, P., Pfeil, B., Pierrot, D., Poulter, B., Rehder, G.,  
459 Resplandy, L., Robertson, E., Rocher, M., Rödenbeck, C., Schuster, U., Schwinger, J.,  
460 Séférian, R., Skjelvan, I., Steinhoff, T., Sutton, A., Tans, P. P., Tian, H., Tilbrook, B.,  
461 Tubiello, F. N., van der Laan-Luijckx, I. T., van der Werf, G. R., Viovy, N., Walker, A. P.,  
462 Wiltshire, A. J., Wright, R., Zaehle, S., and Zheng, B.: Global carbon budget 2018. *Earth  
463 Syst. Sci. Data*, 10, 405, 2018.



- 464 Li, G., Han, H., Du, Y., Hui, D., Xia, J., Niu, S., Li, X., and Wan, S.: Effects of warming and  
465 increased precipitation on net ecosystem productivity: a long-term manipulative  
466 experiment in a semiarid grassland. *Agric. For. Meteorol.*, 232, 359-366, 2017.
- 467 Luo, Y., and Weng, E.: Dynamic disequilibrium of the terrestrial carbon cycle under global  
468 change. *Trends Ecol. Evol.*, 26, 96-104, 2011.
- 469 Luo, Y., and Zhou, X.: *Soil respiration and the environment*. Elsevier, 2006.
- 470 Marcolla, B., Rödenbeck, C., and Cescatti, A.: Patterns and controls of inter-annual variability  
471 in the terrestrial carbon budget. *Biogeosciences*, 14, 3815-3829, 2017.
- 472 Musavi, T., Migliavacca, M., Reichstein, M., Kattge, J., Wirth, C., Black, T. A., Janssens, I.,  
473 Knohl, A., Loustau, D., Rouspard, O., Varlagin, A., Rambal, S., Cescatti, A., Gianelle, D.,  
474 Kondo, H., Tamrakar, R., and Mahecha, M. D.: Stand age and species richness dampen  
475 interannual variation of ecosystem-level photosynthetic capacity. *Nat. Ecol. Evol.*, 1,  
476 0048, 2017.
- 477 Niu, S., Fu, Z., Luo, Y., Stoy, P. C., Keenan, T. F., Poulter, B., Zhang, L., Piao, S., Zhou, X.,  
478 Zheng, H., Han, J., Wang, Q., and Yu, G.: Interannual variability of ecosystem carbon  
479 exchange: From observation to prediction. *Global Ecol. Biogeogr.*, 26, 1225-1237, 2017.
- 480 Novick, K. A., Oishi, A. C., Ward, E. J., Siqueira, M. B., Juang, J. Y., and Stoy, P. C.: On the  
481 difference in the net ecosystem exchange of CO<sub>2</sub> between deciduous and evergreen  
482 forests in the southeastern United States. *Glob. Change Biol.*, 21, 827-842, 2015.
- 483 Oleson, K. W., Lawrence, D. M., Bonan, G. B., Drewniak, B., Huang, M., Koven, C. D., Levis,  
484 S., Li, F., Riley, W. J., Subin, Z. M., Swenson, S. C., Thornton, P. E., Bozbiyik, A., Fisher,  
485 R., Heald, C. L., Kluzek, E., Lamarque, J.-F., Lawrence, P. J., Leung, L. R., Lipscomb, W.,  
486 Muszala, S., Ricciuto, D. M., Sacks, W., Sun, Y., Tang, J., and Yang, Z.-L.: Technical  
487 description of version 4.5 of the Community Land Model (CLM), NCAR Earth System  
488 Laboratory-Climate and Global Dynamics Division, Boulder, Colorado, USA, Tech. Rep.  
489 TN-503+STR, [http://www.cesm.ucar.edu/models/cesm1.2/clm/CLM45\\_Tech\\_Note.pdf](http://www.cesm.ucar.edu/models/cesm1.2/clm/CLM45_Tech_Note.pdf)  
490 (last access: 27 September 2017), 2013.
- 491 Pastorello, G., Papale, D., Chu, H., Trotta, C., Agarwal, D., Canfora, E., Baldocchi, D., and  
492 Torn, M.: A new data set to keep a sharper eye on land-air exchanges. *Eos*, 98, 2017.
- 493 Peng, S., Ciais, P., Chevallier, F., Peylin, P., Cadule, P., Sitch, S., Piao, S., Ahlström, A.,  
494 Huntingford, C., Levy, P., Li, X., Liu, Y., Lomas, M., Poulter, B., Viovy, N., Wang, T.,  
495 Wang, X., Zaehle, S., Zeng, N., Zhao, F., and Zhao, H.: Benchmarking the seasonal cycle  
496 of CO<sub>2</sub> fluxes simulated by terrestrial ecosystem models. *Global Biogeochem. Cy.*, 29,  
497 46-64, 2015.
- 498 Peylin, P., Law, R. M., Gurney, K. R., Chevallier, F., Jacobson, A. R., Maki, T., Niwa, Y., Patra,  
499 P. K., Peters, W., Rayner, P. J., Rödenbeck, C., van der Laan-Luijkx, I. T., and Zhang, X.:  
500 Global atmospheric carbon budget: results from an ensemble of atmospheric CO<sub>2</sub>  
501 inversions. *Biogeosciences*, 10, 6699-6720, 2013.
- 502 Poulter, B., Frank, D., Ciais, P., Myneni, R. B., Andela, N., Bi, J., Broquet, G., Canadell, J. G.,



- 503 Chevallier, F., Liu, Y. Y., Running, S. W., Sitch, S., and van der Werf, G. R.: Contribution  
504 of semi-arid ecosystems to interannual variability of the global carbon cycle. *Nature*, 509,  
505 600-603, 2014.
- 506 Randerson, J. T.: Climate science: Global warming and tropical carbon. *Nature*, 494, 319-320,  
507 2013.
- 508 Randerson, J. T., Chapin III, F. S., Harden, J. W., Neff, J. C., and Harmon, M. E.: Net  
509 ecosystem production: a comprehensive measure of net carbon accumulation by  
510 ecosystems. *Ecol. Appl.*, 12, 937-947, 2002.
- 511 R Development Core Team.: R: A Language and Environment for Statistical Computing  
512 3-900051-07-0, R Foundation for Statistical Computing, Vienna, Austria, 2011.
- 513 Reichstein, M., Bahn, M., Mahecha, M. D., Kattge, J., and Baldocchi, D. D.: Linking plant and  
514 ecosystem functional biogeography. *Proc. Natl Acad. Sci. USA*, 111, 13697-13702, 2014.
- 515 Reichstein, M., Falge, E., Baldocchi, D., Papale, D., Aubinet, M., Berbigier, P., Bernhofer, C.,  
516 Buchmann, N., Gilmanov, T., Granier, A., Grünwald, T., Havránková, K., Ilvesniemi, H.,  
517 Janous, D., Knohl, A., Laurila, T., Lohila, A., Loustau, D., Matteucci, G., Meyers, T.,  
518 Miglietta, F., Ourcival, J., Pumpanen J., Rambal, S., Rotenberg, E., Sanz, M., Tenhunen,  
519 J., Seufert, G., Vaccari, F., Vesala, T., Yakir, D., and Valentini, R.: On the separation of net  
520 ecosystem exchange into assimilation and ecosystem respiration: review and improved  
521 algorithm. *Glob. Change Biol.*, 11, 1424-1439, 2005.
- 522 Richardson, A. D., Keenan, T. F., Migliavacca, M., Ryu, Y., Sonnentag, O., and Toomey, M.:  
523 Climate change, phenology, and phenological control of vegetation feedbacks to the  
524 climate system. *Agric. For. Meteorol.*, 169, 156-173, 2013.
- 525 Rödenbeck, C., Zaehle, S., Keeling, R., and Heimann, M.: How does the terrestrial carbon  
526 exchange respond to inter-annual climatic variations? *Biogeosciences*, 15, 2481-2498,  
527 2018.
- 528 Sakschewski, B., von Bloh, W., Boit, A., Rammig, A., Kattge, J., Poorter, L., Peñuelas, J., and  
529 Thonicke, K.: Leaf and stem economics spectra drive diversity of functional plant traits in  
530 a dynamic global vegetation model. *Glob. Change Biol.*, 21, 2711-2725, 2015.
- 531 Scheffer, M., Bascompte, J., Brock, W. A., Brovkin, V., Carpenter, S. R., Dakos, V., Held, H.,  
532 van Nes, E. H., Rietkerk, M., and Sugihara, G.: Early-warning signals for critical  
533 transitions. *Nature*, 461, 53-59, 2009.
- 534 Valentini, R., Matteucci, G., Dolman, A. J., Schulze, E. D., Rebmann, C. J. M. E. A. G., Moors,  
535 E. J., Granier, A., Gross, P., Jensen, N. O., Pilegaard, K., Lindroth, A., Grelle, A.,  
536 Bernhofer, C., Grünwald, T., Aubinet, M., Ceulemans, R., Kowalski, A. S., Vesala, T.,  
537 Rannik, Ü., Berbigier, P., Loustau, D., Guðmundsson, J., Thorgeirsson, H., Ibrom, A.,  
538 Morgenstern, K., Clement, R., Moncrieff, J., Montagnani, L., Minerbi S., and Jarvis, P. G.:  
539 Respiration as the main determinant of carbon balance in European forests. *Nature*, 404,  
540 861-865, 2000.
- 541 Von Buttlar, J., Zscheischler, J., Rammig, A., Sippel, S., Reichstein, M., Knohl, A., Jung, M.,



- 542 Menzer, O., Arain, M., Buchmann, N., Cescatti, A., Geinelle, D., Kiely, G., Law, B.,  
543 Magliudo, V., Margolis, H., McCaughey, H., Merbold, L., Migliavacca, M., Montagnani,  
544 L., Oechel, W., Pavelka, M., Pelchl, M., Rambal, S., Raschi, A., Scott, R.L., Vaccari, F.,  
545 Van Gorsel, E., Varlagin, A., Wohlfahrt, G., and Mahecha, M.: Impacts of droughts and  
546 extreme temperature events on gross primary production and ecosystem respiration: a  
547 systematic assessment across ecosystems and climate zones. *Biogeosciences*, 15,  
548 1293-1318, 2017.
- 549 Xia, J., Chen, J., Piao, S., Ciais, P., Luo, Y., and Wan, S.: Terrestrial carbon cycle affected by  
550 non-uniform climate warming. *Nat. Geosci.*, 7, 173-180, 2014.
- 551 Xia, J., McGuire, A. D., Lawrence, D., Burke, E., Chen, G., Chen, X., Delire, C., Koven, C.,  
552 MacDougall, A., Peng, S., Rinke, A., Saito, K., Zhang, W., Alkama, R., Bohn, T. J., Ciais,  
553 P., Decharme, B., Gouttevin, I., Hajima, T., Hayes, D. J., Huang, K., Ji, D., Krinner, G.,  
554 Lettenmaier, D. P., Miller, P. A., Moore, J. C., Smith, B., Sueyoshi, T., Shi, Z., Yan, L.,  
555 Liang, J., Jiang, L., Zhang, Q., and Luo, Y.: Terrestrial ecosystem model performance in  
556 simulating productivity and its vulnerability to climate change in the northern permafrost  
557 region. *J. Geophys. Res.-Biogeo.*, 122, 430-446, 2017.
- 558 Xia, J., Niu, S., Ciais, P., Janssens, I. A., Chen, J., Ammann, C., Arain, A., Blanken, P. D.,  
559 Cescatti, A., Bonal, D., Buchmann, N., Curtis, P. S., Chen, S., Dong, J., Flanagan, L. B.,  
560 Frankenberg, C., Georgiadis, T., Gough, C. M., Hui, D., Kiely, G., Li, J., Lund, M.,  
561 Magliulo, V., Marcolla, B., Merbold, L., Montagnani, L., Moors, E. J., Olesen, J. E., Piao,  
562 S., Raschi, A., Rouspard, O., Suyker, A. E., Urbaniak, M., Vaccari, F. P., Varlagin, A.,  
563 Vesala, T., Wilkinson, M., Weng, E., Wohlfahrt, G., Yan, L., and Luo, Y.: Joint control of  
564 terrestrial gross primary productivity by plant phenology and physiology. *Proc. Natl Acad.*  
565 *Sci. USA*, 112, 2788-2793, 2015.
- 566 Yu, G., Chen, Z., Piao, S., Peng, C., Ciais, P., Wang, Q., Li, X., and Zhu, X.: High carbon  
567 dioxide uptake by subtropical forest ecosystems in the East Asian monsoon region. *Proc.*  
568 *Natl Acad. Sci. USA*, 111, 4910-4915, 2014.
- 569 Zeng, N., Zhao, F., Collatz, G. J., Kalnay, E., Salawitch, R. J., West, T. O., and Guanter, L.:  
570 Agricultural Green Revolution as a driver of increasing atmospheric CO<sub>2</sub> seasonal  
571 amplitude. *Nature*, 515, 394-397, 2014.
- 572 Zhao, J., Peichl, M., Öquist, M., and Nilsson, M. B.: Gross primary production controls the  
573 subsequent winter CO<sub>2</sub> exchange in a boreal peatland. *Glob. Change Biol.*, 22, 4028-4037,  
574 2016.
- 575 Zhou, S., Zhang, Y., Ciais, P., Xiao, X., Luo, Y., Caylor, K. K., Huang, Y., and Wang, G.:  
576 Dominant role of plant physiology in trend and variability of gross primary productivity  
577 in North America. *Sci. Rep.*, 7, 41366, 2017.
- 578